PAPER • **OPEN ACCESS**

Optical emission from a ‘beam mode’ transparent cathode glow discharge

To cite this article: T Hardiment and M D Bowden 2021 *Plasma Sources Sci. Technol.* **30** 075010

View the article online for updates and enhancements.

HIDEN ANALYTICAL

Instruments for **Advanced Science**

- Knowledge,
- Experience,
- Expertise

Click to view our product catalogue

Contact Hiden Analytical for further details:

W www.HidenAnalytical.com

E info@hiden.co.uk

Gas Analysis

- dynamic measurement of reaction gas streams
- catalysis and thermal analysis
- molecular beam studies
- dissolved species probes
- fermentation, environmental and ecological studies

Surface Science

- UHV TPD
- SIMS
- end point detection in ion beam etch
- elemental imaging - surface mapping

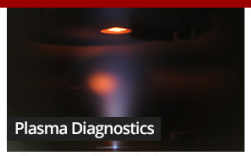

Plasma Diagnostics

- plasma source characterization
- etch and deposition process reaction kinetic studies
- analysis of neutral and radical species

Vacuum Analysis

- partial pressure measurement and control of process gases
- reactive sputter process control
- vacuum diagnostics
- vacuum coating process monitoring

This content was downloaded from IP address 86.167.1.29 on 07/07/2021 at 15:35

OPEN ACCESS
IOP Publishing
Plasma Sources Science and Technology
Plasma Sources Sci. Technol. **30** (2021) 075010 (15pp)
https://doi.org/10.1088/1361-6595/ac0b57

Optical emission from a 'beam mode' transparent cathode glow discharge

T Hardiment and M D Bowden*

Dept. Electrical Engineering and Electronics, University of Liverpool, Liverpool. L69 3GJ, United Kingdom

E-mail: t.hardiment@liverpool.ac.uk and mark.bowden@liverpool.ac.uk

Received 18 March 2021, revised 9 June 2021
Accepted for publication 15 June 2021
Published 7 July 2021

Abstract

We investigate optical emission from a low-pressure 'beam mode' inertial electrostatic confinement glow discharge, created using cylindrical grid electrodes, having cathode inside a grounded, concentric anode. Spectral line distributions were measured in helium from this and a hollow cathode mode, with four lines emitted from singlet and triplet states with $n = 3$ and $L =$ P and D compared against simple models for impact excitation by electrons and by ions and neutrals, suggesting much beam mode emission is caused by fast neutrals, and a significant component also caused by electrons. Beam mode emission occurs in a pattern of radial lines, that pass through aligned electrode apertures and extend across the chamber. Shadows cast by the electrode wires indicate electrically-neutral, beam-like sources of excitation, that cross the electrode assembly from bright radial lines in the opposing inter-electrode space, and calculated potential distributions show lensing surfaces around the anode grid apertures, focussing for inward-drifting ions. These indicate the emission pattern is caused by radially-convergent ion beams, and co-linear beams of fast neutrals produced in these. Emission was also observed with various alterations made to the electrode arrangement: with the anode removed, no beams were observed; with the cathode apertures rotated out of phase with those of the anode, bright radial beams between the electrodes followed the distribution of anode apertures; similar beams appeared with the grid cathode replaced by a solid version. In these experiments, progressive obstruction of pathways through the cathode caused increasing reduction in the beam pattern of emission beyond the anode radius, and in discharge perveance at similar pressure and voltage. Beam-like emission was also observed for a parallel-planar configuration, in which a cathode grid was held between two identical anode grids. The beam mode is shown to be a convergent, anode-focussed ion beam discharge, distinct to the star mode described elsewhere.

Keywords: inertial electrostatic confinement, glow discharge, optical emission, helium spectroscopy, ion beams, grid focussing, fast neutrals

(Some figures may appear in colour only in the online journal)

1. Introduction

The beam mode is a low-pressure glow discharge producing a characteristic beam-like pattern of light. It occurs in an inertial electrostatic confinement (IEC) device with a coaxial arrangement of cylindrical wire-grid electrodes, in which a central cathode is biased to a high DC voltage. We have previously described [1, 2] how the beam mode operates at pressures too low for a hollow cathode mode to sustain, and also how the principal colour of optical emission from the beam mode in helium indicates collisional processes that are caused significantly by energetic ions and neutrals. In this paper we shall further examine this unusual emission spectrum, and

* Author to whom any correspondence should be addressed.

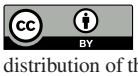

Original content from this work may be used under the terms of the Creative Commons Attribution 4.0 licence. Any further distribution of this work must maintain attribution to the author(s) and the title of the work, journal citation and DOI.

investigate how the beam-like form of the discharge relies upon physical properties of the experimental set-up.

Glow discharges in which ions and neutrals are significantly energetic are relatively uncommon, and have mostly been studied in IEC for non-power fusion applications. Early IEC work was conducted at lower pressures [3–6], but since a simple discharge source was developed at the University of Illinois in the 1990s [7–11] research has been directed towards better understanding and improving the efficiency of benchtop fusion devices [12–31], since near-term applications increase with performance. These generally use a spherical or cylindrical hollow wire-grid cathode, operated either as self-sustained 'transparent cathode' discharge (TCD) or with an ionisation source. Aside from fusion, energetic 'heavy particle' discharges have been considered for relatively few other applications. Ions become energetic at conditions of high electric field to gas density ratio (E/N), and resonant charge-exchange can produce significant numbers of fast neutrals [32–37]. Using a TCD as fast neutral source has been proposed for a thruster [38], and might be considered for further neutral beam applications such as materials processing e.g. [39–41]. For other technological applications, the possible advantages of accessing a different, heavy particle-impact collisional regime are largely unexplored.

A primary interest for work directed towards any of these applications lies in the understanding of fundamental processes by which discharges operate, and how these depend upon physical properties of the device. To investigate processes occurring in the beam mode discharge, we compare principal characteristics of the emission spectrum observed for different modes in helium with general features of the cross section structure for excitation by electrons, ions and neutrals. We also examine the spatial distribution of emission, in which radial spoke-like lines pass through the electrode apertures, resembling the characteristic appearance of the 'star' mode discharge reported for many other spherical and cylindrical IEC devices [8, 10, 18, 22, 28, 42, 43]. We are interested in how this distribution is determined by our electrode configuration, which is unusual for an IEC set-up in having a relatively short, open-ended cathode grid surrounded by a relatively closely-spaced anode grid, with apertures of each arranged in radial alignment. We investigate by making a series of alterations to the electrode arrangement and observing the effect upon emission. Details of the experimental apparatus are described in section 2, and results of our experiments are described and analysed in section 3, and discussed in section 4.

2. Experimental apparatus and procedure

2.1. Vacuum system and power supplies

The discharges were created in a cube-shaped vacuum chamber, with 30 cm sides. The floor and walls of this are stainless steel, and the top is acrylic, with glass to shield against high temperature particle fluxes and x-ray emission. Various ports located upon each side of the chamber are used for services, diagnostics and viewing windows. The system is evacuated with a Leybold Turbovac50 turbo-molecular pump backed by an Edwards RV3 rotary pump. High-purity research grade gas was used for all experiments, admitted with MKS GE50A series mass flow controllers, with pressure monitored using a Pfeiffer CMR375 capacitance manometer. Extrapolating the relation between gas flow and pressure down to the base pressure of around 10^{-3} Pa provides an idea of leak rate and so background gas purity in the chamber, which we estimate to remain greater than 98% for all experimental conditions. The cathode was biased negative from chamber ground using a DC high voltage power supply. A Glassman WX series unit was available for some experiments, rated for 35 mA at voltages up to 30 kV. At other times a smaller unit from 3B Scientific was used, with current limited to 2 mA at voltages up to 6 kV.

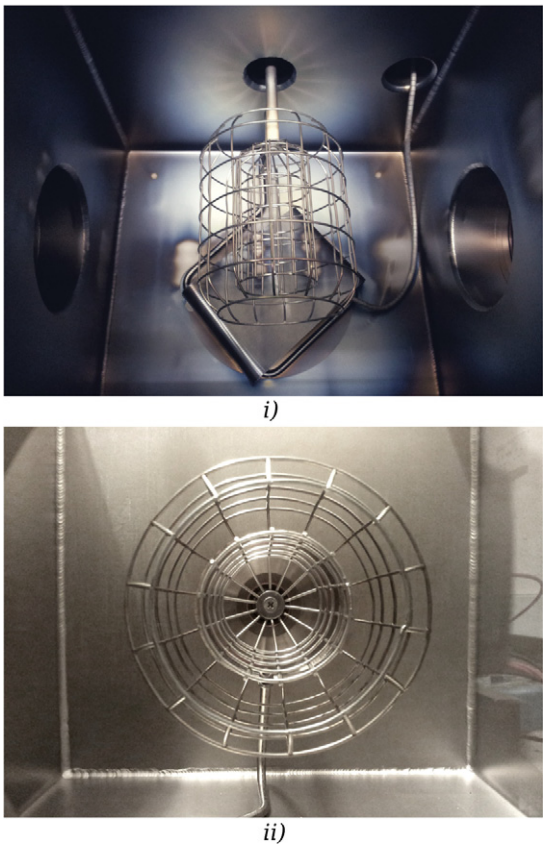

Figure 1. Photographs showing standard electrode assembly within the vacuum chamber, taken from (i) an elevated perspective with chamber open and (ii) through an axial viewport.

2.2. Electrodes

Photographs of our standard electrode arrangement, used for experiments described in sections 3.1 and 3.2, are shown in figure 1. Cylindrical grid electrodes are positioned with cathode inside the anode. The anode radius is around 5.6 cm, twice the cathode radius, making the inter-electrode separation equal to the cathode radius of around 2.8 cm. Both electrodes are made from 1.6 mm diameter stainless steel wire. Welded 2.5 cm square mesh was formed into cylinders, with an extra set of longitudinal wires added to the cathode, so that both electrodes have 14 rows of apertures spaced evenly around the circumference. The electrodes are arranged with apertures

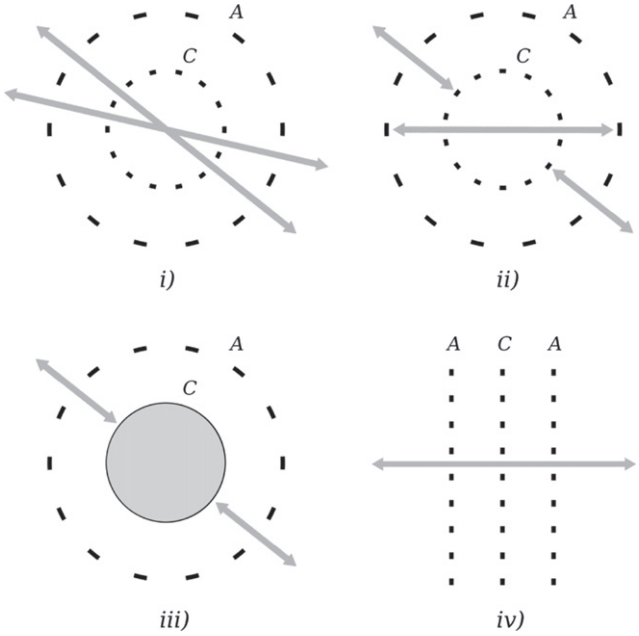

Figure 2. Diagrams from axial perspective showing (i) standard electrode arrangement, and modified configurations with (ii) rotated cathode, (iii) solid cathode, and (iv) planar grids. The letters A and C indicate anode and cathode respectively, arrows indicate available perpendicular pathways through the assemblies.

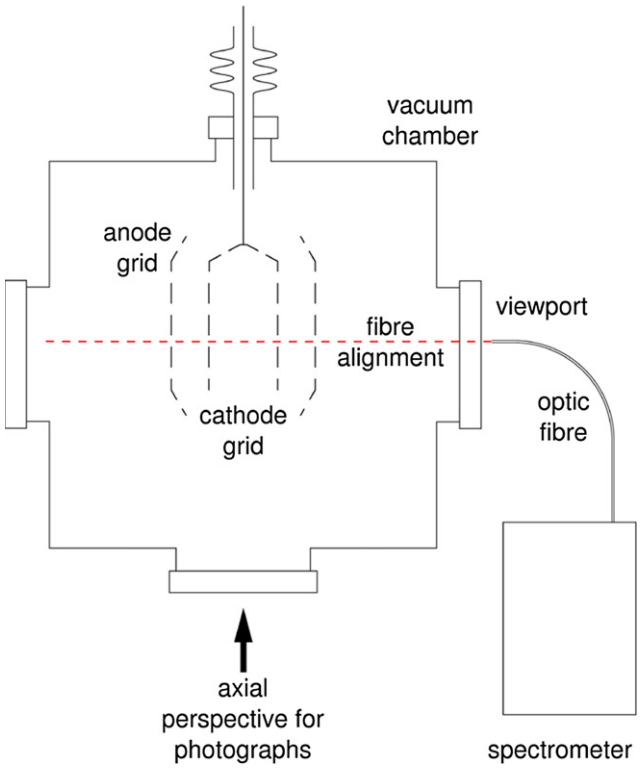

Figure 3. Chamber plan showing apparatus used for optical measurements in section 3.1, and the axial perspective used for many photographs in sections 3.2 and 3.3.

in radial alignment allowing clear diametric paths through the anode–cathode assembly, as shown in the diagram of figure 2(i). There are four bands of apertures along the 10 cm cathode length. The anode has an additional row of apertures at each end, angled to around 80% of the main radius, and is held close to chamber ground by a small resistance, so both this and the chamber wall act as anode for the discharge. One end of the cathode grid cylinder is open to the chamber volume, while the other end is attached to the high voltage feed-through stalk by supporting wires.

We also observed distributions of emission in a series of different electrode arrangements, that were designed to modify specific properties of the standard apparatus. In a 'rotated cathode' configuration, the cathode was rotated about its axis so that the apertures of anode and cathode were arranged in anti-phase, causing grid wires to intersect radial pathways through the electrodes as shown in figure 2(ii). Two further assemblies, shown in figures 2(iii) and (iv), retain different properties of our usual set-up while removing the physical space enclosed by the cathode, that is typically found in IEC devices. In one of these (figure 2(iii)), a solid-surface stainless steel cathode of similar dimensions was substituted for the standard grid. This 'solid cathode' arrangement retained both the cylindrical format and the anode grid from the standard apparatus, while removing any effect of cathode apertures and/or diametric paths through the device. In a second version, perpendicular paths through a multiple-grid set-up were preserved by replacing the cylindrical assembly with a parallel-planar arrangement, in which a single cathode grid was held between a pair of identical grounded anode grids (figure 2(iv)). These electrodes were made from 16 cm circles cut from square stainless steel mesh, having pitch a little smaller than 1 cm to increase uniformity across the plane of the electrodes, and wire diameter around 1 mm. The inter-electrode separation was 2 cm.

2.3. Diagnostics

A diagram in figure 3 shows the basic experimental layout. For measurements of optical emission, light was collected using an ocean optics UV–Vis optic fibre to a Horiba FHR1000 monochromator. The output of this was monitored with a Hamamatsu R928 photomultiplier (PM) tube, and recorded on a computer. For recording spatial distributions of emission we used standard imaging cameras, and have made minor adjustments to individual images where variations in colour rendition were distracting. Any more significant manipulation is described in the text. Details of experimental procedures are described in section 3.

3. Results and analysis

Before concentrating upon optical emission from the beam mode, we first summarise some general procedures and operating characteristics described in previous work [1, 2].

Discharges used for the experiments are created by first evacuating the chamber and backfilling to a given operating pressure, then increasing cathode voltage until breakdown occurs. For pressures below a few tens of Pascals, the discharge mode structure is significantly determined by conditions at

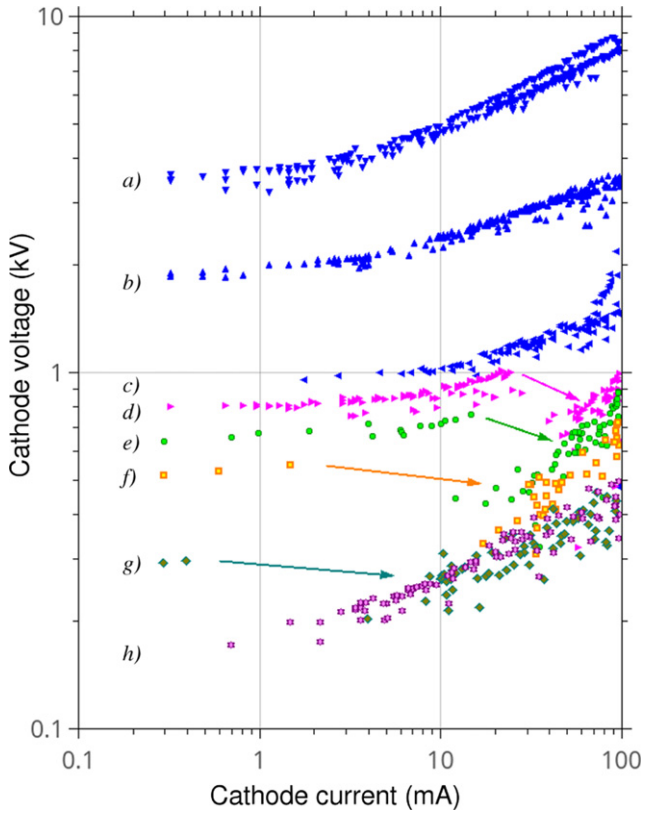

Figure 4. Current–voltage curves for helium discharges at pressures: (a) 3.9 Pa; (b) 6.1 Pa; (c) 11.7 Pa; (d) 12.8 Pa; (e) 14.8 Pa; (f) 18.7 Pa; (g) 32 Pa; (h) 85 Pa. Arrows indicate jumps in current and voltage on instigation of the CC mode. Figure reproduced from © [2019] IEEE. Reprinted, with permission, from [1].

which a hollow cathode mode may sustain within the cathode cavity. This may be seen in the current–voltage curves for helium discharges reproduced in figure 4. At higher pressures the hollow cathode mode occurs at breakdown, as in the curve for 85 Pa marked (h) on the figure. For pressures $35 \gtrsim p \gtrsim 12$ Pa (curves (d)–(g)) the discharge may operate in either the hollow cathode mode, or a higher-impedance mode in which much emission is located along the axial line between open cathode end and chamber wall. The points of transition between these modes are evident as discontinuities in the current–voltage curves, that are marked with arrows. The high-impedance mode seems analogous to the 'high voltage' conventional hollow cathode mode described in the literature [44, 45]. Over a range of increasingly lower pressures in our apparatus, in helium over pressures $p \gtrsim 7$ Pa, we observe this state to undergo a progressive change in spatial distribution of emission in which the axial glow becomes a narrow, fainter beam, and the pattern of radial lines characteristic of the beam mode develops. For pressures $p < 7$ Pa the beam mode discharge remains similar in appearance at the lowest pressure tested, which was around 2 Pa, requiring cathode voltage V_C of ~30 kV. In helium the axial and radial spatial elements are associated with distinct colours, with the hollow cathode and axial glow a bright green and the radial emission pale orange. Photographs showing spatial distributions of emission for some transitional states over this range can be found in our previous studies [1, 2]. The colour variation results from emission at different principal wavelengths, that correspond with large respective cross sections for excitation by electrons and ions, indicating different sets of collisional processes in the two modes caused by electrons and heavy particles. While we have concentrated upon helium discharges, a similar mode structure observed at slightly different pressure ranges for other gas species shows this progression to be quite general. At beam mode conditions operating voltages rise significantly with reduction in pressure. Before making measurements, the discharge was operated for some minutes to let conditions stabilise, since after breakdown a sharp rise and more gradual decay in pressure would be accompanied by significant variation in cathode voltage and current. This was observed for various degrees of chamber conditioning, although a larger magnitude after the chamber had been opened suggests a relation with gas desorption from internal surfaces. Our observations were made for discharges operating at generally stable conditions, and where drift occurred over longer measurement periods, small gas flow adjustments were made to maintain consistent levels of voltage and current.

In the following we treat different aspects of beam mode optical emission separately. We first consider the wider spectrum of visible emission from helium discharges in part 3.1, before examining the spatial distribution of emission observed using our standard electrodes in part 3.2. Observations made with different arrangements are described in part 3.3.

3.1. Spectral emission in helium

For a broad overview of the helium emission structure, we measured wavelengths between 250 nm and 750 nm from discharges operating at various pressures over the range $p = 3$–50 Pa. We note that for measurements made at pressures $p > 15$ Pa, the discharge was operating in the hollow cathode mode with $V_C = 200$–400 V, and at pressures $p < 7$ Pa measurements were made of the beam mode, with V_C of a few kV up to around 20 kV. For all of these, light was sampled using an optic fibre held in a fixed position, as shown in figure 3. This was a short distance from a viewport with no lead glass fitted, and located to one side of the electrodes, so that line of sight was aligned with either a radial beam in the beam mode, or the central hollow cathode mode glow. Some measurements were also made at pressures $7 < p < 15$ Pa, conditions at which elements of both axial and radial glow were sampled. For each measurement, the pressure was set and the discharge left to stabilise. The spectrometer/PM tube system was then used to scan across the full range of wavelengths, while maintaining a consistent voltage at conditions of constant current. This technique enabled the emission structure to be assessed across a wide range of conditions, although for practical interests of integration time, wavelength resolution was limited to 0.25 nm. The degree of error introduced by the sampling interval will differ for individual wavelengths, and so principally affect their relative distribution. We are concerned rather with consistency among results for each spectral line, for which we estimate errors to be generally within 10%, although fainter lines in the spectrum are subject to additional error from noise. Recorded

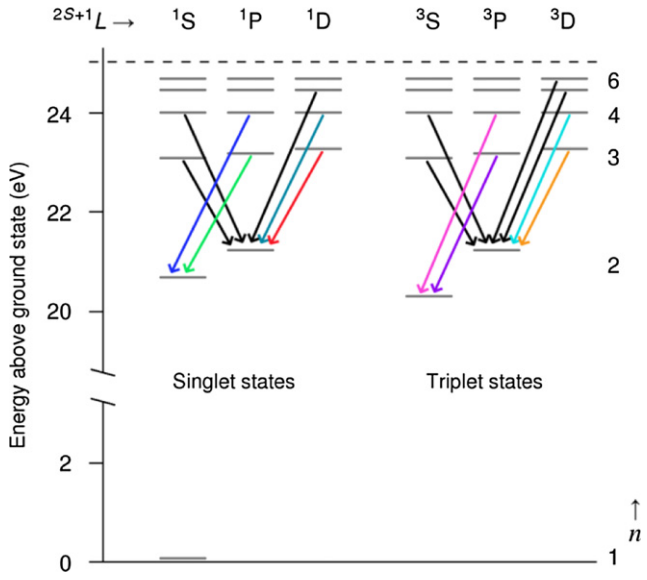

Figure 5. Simple state diagram for helium, showing transitions that cause emission at the observed wavelengths. A key to these is given in table 1. Transitions from levels with $n = 3, 4$ and $L =$ P, D, that emit at wavelengths shown in figure 6, are marked in colour online.

Table 1. Wavelengths of observed helium lines, the electronic transitions causing these, and branching factors B_{jk} that relate emission to excited population of the upper level [46].

Wavelength (nm)	Transition	B_{jk}
318.8	$4^3\text{P} \rightarrow 2^3\text{S}$	1.27
382.0	$6^3\text{D} \rightarrow 2^3\text{P}$	1.50
388.9	$3^3\text{P} \rightarrow 2^3\text{S}$	1.11
396.5	$4^1\text{P} \rightarrow 2^1\text{S}$	35.6
402.6	$5^3\text{D} \rightarrow 2^3\text{P}$	1.39
438.8	$5^1\text{D} \rightarrow 2^1\text{P}$	1.53
447.1	$4^3\text{D} \rightarrow 2^3\text{P}$	1.27
471.3	$4^3\text{S} \rightarrow 2^3\text{P}$	1.61
492.2	$4^1\text{D} \rightarrow 2^1\text{P}$	1.34
501.6	$3^1\text{P} \rightarrow 2^1\text{S}$	43.2
504.8	$4^1\text{S} \rightarrow 2^1\text{P}$	1.69
587.6	$3^3\text{D} \rightarrow 2^3\text{P}$	1.00
667.8	$3^1\text{D} \rightarrow 2^1\text{P}$	1.00
706.5	$3^3\text{S} \rightarrow 2^3\text{P}$	1.00
728.1	$3^1\text{S} \rightarrow 2^1\text{P}$	1.00

line intensities are the sum of values measured for wavelengths across each line, after correction for the fibre transmission and PM tube response.

In the following description, we shall use the notation $n^{2S+1}L$ to refer to specific excited states, where n is principal quantum number and L is orbital angular momentum. $2S + 1$ refers to spin multiplicity, where S is total spin, of 0 for the singlet and 1 for the triplet states.

For conditions across the experimental range, 15 atomic helium lines were consistently observed, that correspond to transitions from singlet and triplet levels with $n = 3$, 4 and $L =$ S, P and D, and also the 5^3D, 5^1D and 6^3D levels. For reference, we have marked the transitions on a simple state diagram in figure 5, and a key to the emitted wavelengths

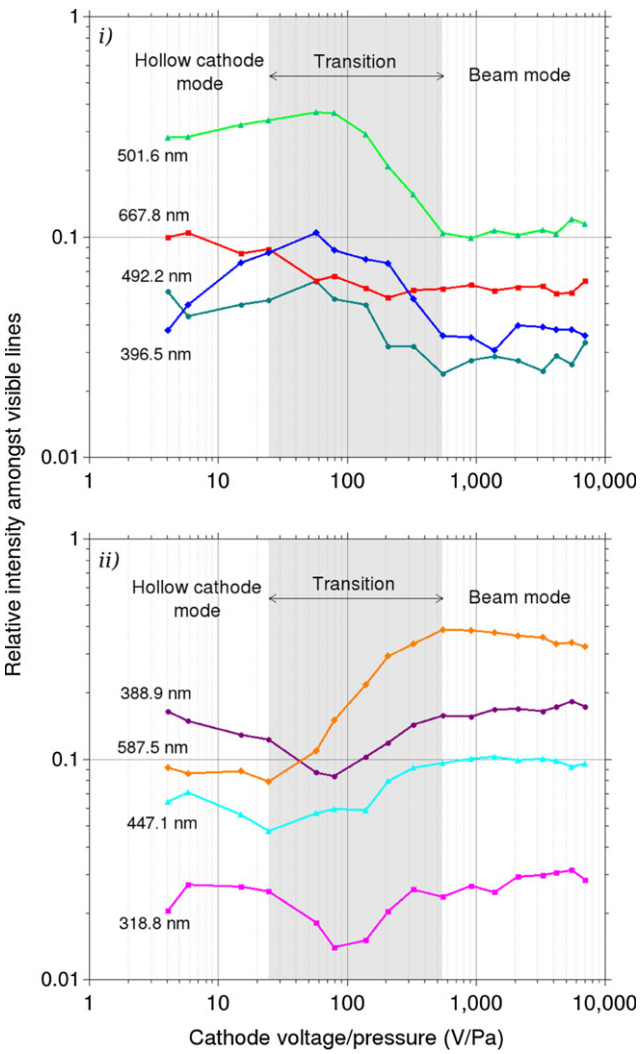

Figure 6. The relative distribution of (i) singlet and (ii) triplet emission, from levels with $n = 3, 4$ and $L =$ P, D, observed for a range of V/p conditions covering operation in both the hollow cathode and beam modes. In the hollow cathode mode 200 V $< V_C <$ 400 V, 50 Pa $> p >$ 16 Pa, and in the beam mode 4 kV $< V_C <$ 20 kV, 7.1 Pa $> p >$ 2.8 Pa.

is given in table 1. No clearly Doppler shifted profiles were evident for these lines, although this is considered inconclusive as we expect spectral line intensities to be significantly influenced by effects of pressure at glow discharge conditions [35, 47–50], causing contributions made by any shifted components to be relatively small. Values measured for lines in the S series were generally smaller than for P or D, which is also consistent with the lesser amplification by pressure expected for these [46]. The S lines, and those from higher D levels, together contributed less than 15% to totals recorded for most conditions, and for clarity these are omitted from results plotted in figure 6, that show the distribution of emission from P and D levels with $n = 3$ and 4. The results for singlet and triplet lines are grouped separately, and plotted against conditions of V/p (where $V = V_C$), for which the ordering of data points corresponds to monotonic increase in voltage and decrease in pressure. These show line intensities within each

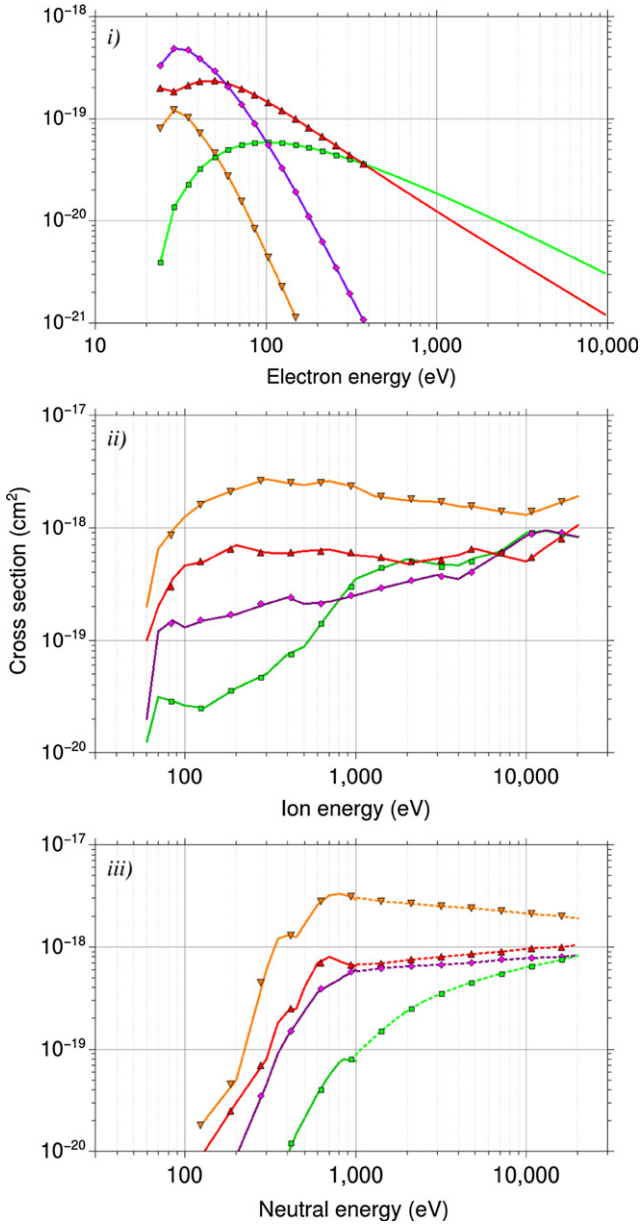

Figure 7. Cross sections for helium emission after excitation by (i) electrons [52], (ii) ions [53] and (iii) neutrals [57] (extrapolations to ion-impact values at 20 keV shown as dashed lines). Wavelengths are indicated as ▽ 587.6 nm, △ 667.8 nm, ◊ 388.9 nm and □ 501.6 nm.

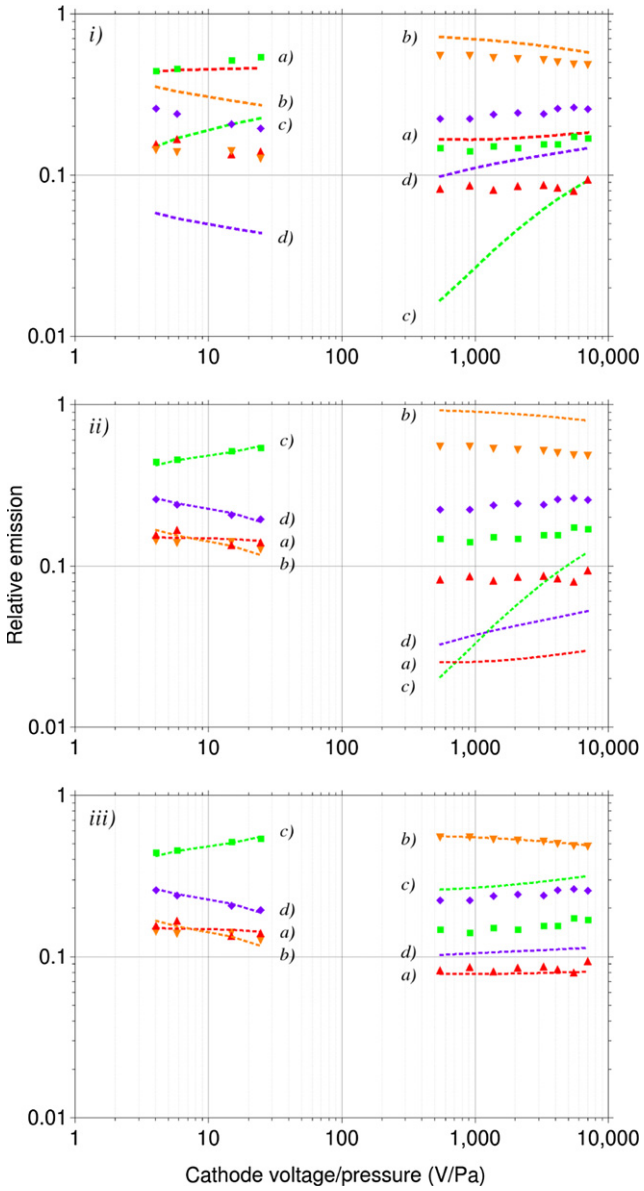

Figure 8. Model results (broken lines) showing (i) directly-excited emission profiles for electrons and heavy particles, (ii) after correction for experimental conditions for electrons and heavy particles, and (iii) emission at experimental conditions for a 45%–55% electron-heavy particle mix. Wavelengths are annotated as (a) 667.8 nm, (b) 587.6 nm, (c) 501.6 nm and (d) 388.9 nm. All results are shown compared with experimental values, indicated by ▽ 587.6 nm, △ 667.8 nm, ◊ 388.9 nm and □ 501.6 nm.

spectral series to follow a broadly similar dependence upon conditions, with those from $n = 3$ states brighter in each case. The significant variation for 501.6 nm and 587.6 nm lines that we observed previously is seen to be part of a wider shift from singlet to triplet emission that occurs from hollow cathode to beam modes. The mode progression is also marked on figure 6, showing most of the change to happen over conditions where the discharge was operating in transitional states, and emission was sampled from elements of both cathode-internal glow and radial beam pattern. For conditions within each mode, most lines follow relatively consistent distributions. Emission from the P singlet series is generally brightest for the hollow cathode mode, this share increasing for conditions of greater voltage/pressure within the range. For the beam mode, the brightest series are the D triplets, with some shift to other lines evident for conditions of greatest voltage/pressure.

These results are consistent with emission profiles caused by different sets of collisional processes in the two modes. Having previously noted the principal wavelengths 501.6 nm and 587.6 nm to correspond with large cross sections to 3^1P and 3^3D for electrons and ions, we examine the extent to which the different emission profiles may be further related to underlying cross section structure. The relation

between observed emission and directly-excited populations is complicated by effects of pressure such as radiation imprisonment [47] and collisional transfer [48], that are known to alter the intensity distribution of spectral lines. Pressure effects however saturate at conditions of sufficient optical depth, which was observed in a medium of a few millimetres of helium at pressures above around 15 Pa [46]. While the beam mode operates at pressures below this, the optical path is longer by a larger factor, and so conditions in our chamber are expected to remain largely opaque across the experimental range. A generally consistent effect of pressure will combine with other wavelength-dependent errors, so that a global correction factor for each wavelength might practically relate observed spectra with levels of emission resulting from direct excitation. The reference data for heavy particle-impact processes is incomplete, but we can make some assumptions regarding energy distribution functions (edfs) to model a limited electron-impact emission profile that might be representative of the hollow cathode mode, and a heavy particle-impact version for conditions that might reasonably occur in the beam mode. The calculated profiles can then be compared with experiment, by applying an identical wavelength-specific correction to each.

To model emission for the hollow cathode mode we consider excitation caused by electrons emitted from the cathode under ion bombardment, sometimes referred to as 'γ-electrons' after the second Townsend coefficient γ. These undergo a pendulum motion in hollow cathode discharges [44, 45, 51], in which they repeatedly cross the central negative glow at high velocity while confined by the surrounding sheath structure. At ideal conditions, all energy available from a cathode fall of similar magnitude to V_C is expended in inelastic processes within the negative glow, that occur over all energies between threshold and eV_C (where e is charge of an electron). At lower pressures this distribution may be affected as γ-electrons escape while still energetic, and multiplication in the cathode fall regions is required for the discharge to sustain. Previous modelling of the hollow cathode mode (using equation (7) in reference [2]) suggested fast electrons born in the sheath contribute less than 10% to ionisation at $V_C = 200$ V, rising to around a quarter by $V_C = 400$ V, and so we expect a largely even distribution of electron energies below eV_C for conditions of the hollow cathode measurements.

For the heavy species, ion edfs in the parent gas are known to be broadly thermal over a very wide range of conditions due to charge exchange collisions, that also produce populations of energetic neutrals with similar temperature to the ions. The charge exchange cross section Q_{CX} varies slowly with energy ϵ, and ion temperature T_i can be reasonably approximated as a function of E/N [32, 36]. We have little direct information about conditions in the beam mode, and so for simplicity assume E/N is proportional to background V/p. This approximates the potential distribution to be qualitatively similar across the range, and the background gas to remain at around room temperature. For a nominal correspondence with experimental conditions we shall consider a 'beam' electric field modelled as 70% of cathode potential falling along a path $d = 5$ cm. Conditions in the real discharge may vary considerably from this, but we expect at least some degree of overlap with the model across the range. For each set of conditions we approximate $T_i = E/NQ_{CX}$ and calculate Maxwellian edfs using $f(\epsilon) = C\exp(-\epsilon/T_i)$ as in equation (3) from reference [36], with a value $Q_{CX} = 1.0 \times 10^{-15}$ cm^2. In reality the energy-dependence of Q_{CX} will affect the relation between T_i and E/N, and inelastic losses and runaway are known to cause some variation from Maxwellian for some conditions. In line with the assumptions made so far, weighting of ion and neutral contributions is determined by the average number of charge exchange collisions occurring over the ion transport distance d, with the neutral component multiplied by a factor dNQ_{CX}. This neglects the possible effect of longer paths for neutrals, and so may underestimate the neutral contribution.

Cross section data covering electron, ion and neutral collisions is available for the singlet and triplet lines emitted from $n = 3$ states, with $L = $ P, D. Some cross sections are for emission at discrete wavelengths $\sigma(j \to k)$, while others are for excitation to upper levels $\sigma(j)$ and are adjusted according to branching factor B_{jk} of transition probabilities from the upper state A_j ($B_{jk} = \sum A_j/A_{jk}$), using values listed in table 1 [46]. This has a principal effect for $\sigma\left(3^1\mathrm{P} \to 2^1\mathrm{S}\right)$ due to the much larger probability for transition to ground, other less significant considerations such as cascade population from higher levels are neglected. Cross sections are shown grouped by species in figures 7(i)–(iii). The electron-impact data are recommended functions taken from reference [52], divided by B_{jk}. For ion-impact we use emission cross sections [53] with the 501.6 nm data reduced by the factor of 8 suggested by the authors to make the set consistent with higher-energy measurements [54, 55], this agreeing also with others not shown [56]. For neutral-impact we considered two sets of cross sections [57, 58], that show qualitative agreement over similar ranges of energies below 1 keV. Those selected [57] are of most similar size to the ion-impact data; the others are greater by around an order of magnitude after authors' corrections [59], and have excitation to 3^1P relatively larger by a factor of around 4. For lines other than 3^3P the energy range covers the rise to first maximum, showing a generally similar distribution to the lower-energy ion-impact data. For 3^3P the cross section is still rising at 1 keV, which might influence the results, since to extend the neutral data to higher energies we have simply extrapolated between 1 keV and the ion-impact values at 20 keV (shown as dashed lines on figure 7(iii)). This approximation follows a general convergence between other ion and neutral processes in the kinetic regime such as ionisation and secondary electron emission [60, 61], and in the absence of further data seems reasonable. The neutral data are also divided by B_{jk}.

Emission distributions were calculated for a series of conditions within each mode, corresponding to conditions at which measurements were made. We did not create continuous functions to approximate the heavy particle cross sections, but took values for discrete energies, as indicated by the markers on the cross section plots in figure 7, and evaluated contributions weighted according to contiguous ranges of energies centred around these. A similar procedure was followed to calculate the electron-impact profile, using energies again indicated by

Table 2. Empirical correction for pressure and transmission, matching modelled emission for the hollow cathode mode with experiment.

Wavelength (nm)	Correction factor
388.9	2.2
501.6	8.1
587.6	8.5
667.8	1.0

the plot markers. The results of these calculations show relative levels of emission predicted to occur from direct excitation, which are compared with experimental data in figure 8(i). The poor agreement evident between these is principally attributed to the large expected influence of pressure, and with more confidence in the data and assumptions used for the hollow cathode model, a trial correction was constructed to match these results with the experimental distribution. For this, it was necessary to scale results by the factors shown in table 2, transforming the profiles as shown in figure 8(ii). Agreement between the heavy particle profile and beam mode emission is deteriorated further by the correction, that projects heavy particle-impact emission to be almost completely dominated by the 587.6 nm line at experimental conditions. We then explored the effect of introducing an electron-impact component to the heavy particle model, using a flat contribution based upon the values calculated for the hollow cathode mode operating at 390 V. The beam mode profile shown in figure 8 (iii) demonstrates how such an electron contribution of around 45% can bring levels of emission at 587.6 nm and 667.8 nm into line with experimental values, although for the P lines the projected share at 501.6 nm is too large, and at 388.9 nm too small, by a factor of around 2 in either case.

Dependences of the results were explored by altering some of the assumptions made. We shall not describe these in much detail, but note the following points. The results were largely unchanged when we added an additional component to the electron edf, peaked towards lower energies to simulate a greater degree of multiplication in the sheath. Any electron losses were neglected, and the addition was sufficient for initial populations of γ-electrons to be approximately doubled by threshold energies. Using this edf required only a minor adjustment, of order 10%, to values in table 2 to match the hollow cathode profile with experiment. The results were also relatively insensitive to use of a different extension of neutral cross sections, where the extrapolated values were replaced with data for 1 keV across all higher energies. This reduced the fall in 587.6 nm emission otherwise predicted across the beam mode range, serving to illustrate how this feature of the profiles in figure 8 rely upon both a fall in cross sections with increasing energy and rise in E/N. For either alteration, an electron component of between 40%–45% was required for similar matching of heavy particle D line results with beam mode measurements to that shown in figure 8(iii). This is considered a reliable indication of a significant element of electron-impact excitation occurring in the beam mode, although given the limitations of the model, and its failure to reproduce some elements of observed emission, the quantity is subject to considerable uncertainty. Future work might seek to observe beam mode emission from well-resolved spatial locations, to determine whether the electron signature originates within the beam, or within the cathode as is visibly apparent for transitional conditions.

To briefly consider reasons for the model's failure to reproduce the distribution of P lines in the beam mode profile, we first note the modelled heavy particle emission relies significantly upon the distribution of neutral-impact cross sections. With little other data available for comparison however, we can only observe these are subject to uncertainty of $\pm 60\%$, that may not fully account for the discrepancy unless the distribution changes significantly over the range of energies 1 keV $< \epsilon <$ 20 keV. A further possibility is for effects of pressure to vary for results from the different modes. While a variation in opacity is known to cause non-linear change in spectral line intensities [46], for such a change to only occur over pressures at the mode transition seems unlikely. A more plausible explanation might be that specific effects of pressure vary somewhat with the collisional profile; since the effective amplification of visible lines is strongly influenced by the spectrum of UV emission from directly-excited populations, any change in this spectrum might be expected to also modify the distribution of visible emission.

3.2. Beam mode emission distribution

We refer to the 'beam' mode because of a beam-like distribution of emission, that has been observed to remain similar in appearance over ranges of conditions in various gas species [1, 2]. This is illustrated with photographs of beam mode discharges in our standard electrode arrangement in figure 9 (see also figures 1 and 2(i)). These show discharges operating at pressures of $p = 3$–4 Pa in helium, with cathode voltage and current of $V_C = 8$–15 kV and $I_C = 10$–20 mA. From the discharge axis (figure 9(i)) emission appears principally along bright radial lines, that pass through apertures of both electrodes and cross the axis. The beams appear brighter and more focussed within the anode radius, and the pattern also extends out into the chamber, where additional straight dark lines are just visible between brighter parts of the beam pattern. The perspective is not precisely axial, but where the radial features are best aligned the bright lines of emission in the inter-electrode region can be seen to be only a millimetre or two in diameter. From an angle, as in figure 9(ii), one beam can be seen to be associated with each pair of radially aligned apertures. The photograph in figure 9(iii) shows the discharge from above, where we observe much of the beam emission to be associated with the central two bands of electrode apertures. We also show another image from the axial perspective, in figure 9(iv), of the discharge after a mechanical failure disturbed the concentric alignment of the electrodes (for the other axial view, in figure 9(i)), the electrodes are generally well-aligned, although an irregularity in the end ring of the anode makes this appear less so). In figure 9(iv), the anode has dropped and turned relative to the cathode, which can be seen to cause a splitting effect for beams on the right of the image. In previous descriptions of these discharges [1, 2] we noted characteristic emission occurring along the axial line between open cathode end and cham-

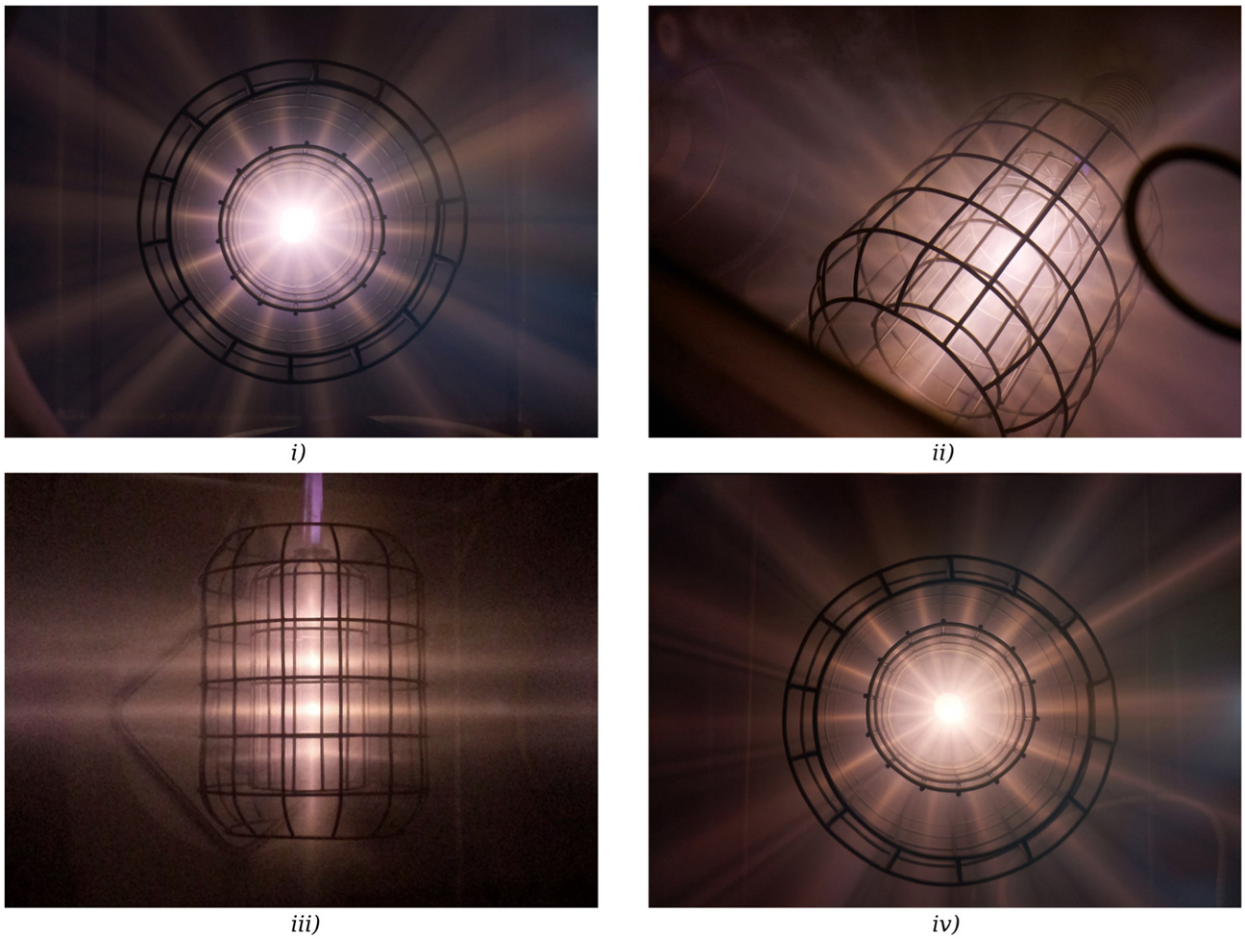

Figure 9. Photographs of beam mode discharges in helium, operating in the standard electrode arrangement at similar discharge conditions of between 3–4 Pa, 8–15 kV and 10–20 mA. Images (i)–(iii) show the discharge from different perspectives, and (iv) shows the effect of electrode misalignment, as described in the text.

ber wall, that in helium evolves from a bright green plume to a fainter narrow beam over pressures $p = 15$–5 Pa. This axial beam emission is quite faint for conditions illustrated in figure 9, and not particularly evident in the photographs.

To clarify details of the distribution from the axial perspective, levels of contrast were enhanced for the image of figure 9(i). Brightness varies considerably for different regions within the original photograph, and so these were manipulated separately. The results in figure 10 reveal an extensive pattern of thin straight dark lines, that is most clearly visible in the region surrounding the left side of the anode grid, between the bright radial bands of emission. This is largely made up of twin lines diverging radially from the locations of longitudinal wires around the anode circumference. We have further illustrated the geometry of these features by marking the extension of four such lines in the upper left quadrant of the figure with broken black and white. This shows the lines in each pair to be oriented towards the approximate centres of adjacent anode apertures situated on the far side of the apparatus. Other, single dark line features are also visible within brighter parts of the radial distribution. In contrast to the twin lines, these extend within the anode radius to intersect with longitudinal wires of the cathode, such as the two examples indicated with arrows in figure 10.

The dark lines consistently extend outward from locations of longitudinal electrode wires, indicating this to be a grid-shadowing effect in the emission surrounding the electrodes. This implies a source for the shadowed emission that is both beam-like, and arranged in distinct components, in order to cast multiple shadows from single wires. The geometry and orientation of these shadows are consistent with a series of radial beams, that have crossed the axis from points of origin within the anode apertures, with the twin lines appearing where fringe elements of adjacent beams are both incident upon the opposing anode wire. The orientation of single lines of shadow is consistent with obstruction by cathode wires of the same beams, that are indicated to cause much of the radial pattern of emission. The shadows appear similarly unperturbed by electrodes of either polarity, indicating the shadowed emission to result from excitation by a series of fast neutral beams, that have crossed the assembly in principal alignment with the bright lines of radial emission in the inter-electrode region. As apparent sources of both fast neutrals and local emission, these inter-electrode beams are implied to be locations of energetic ion transport across the potential fall. This interpretation

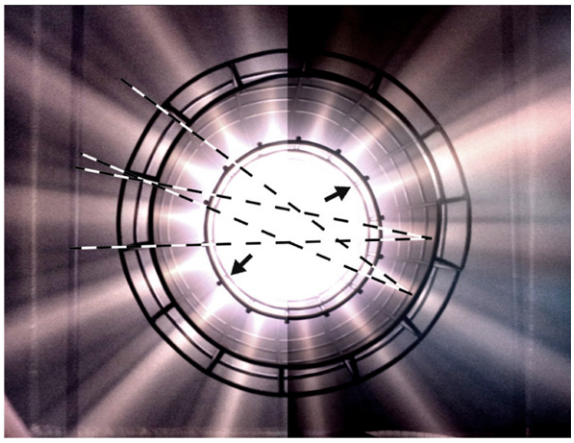

Figure 10. Image of helium discharge from figure 9(i) with contrast levels enhanced. Black and white dashes illustrate geometry of shadows cast by longitudinal members of the anode, arrows indicate examples of cathode shadowing.

might also explain the beam-splitting effect observed for the misaligned electrodes shown in figure 9(iv). In the example at roughly the 2 o'clock position, the lower component does not project beyond the anode and remains aligned with the centre of an anode aperture, consistent with emission produced by a beam of ions converging towards the axis. The upper part however appears to extend from the opposite anode aperture, and to follow a trajectory that is no longer aligned with the displaced anode. This continues beyond the anode to the wall, consistent with a fast neutral beam that has crossed the apparatus.

The influence of the anode grid in our set-up was investigated by comparing radial potential distributions for assemblies both with and without the anode, that were calculated for vacuum conditions with modelling software. In an operating discharge, charged particles may cause local potential to be altered significantly from these, but it is nonetheless interesting to observe the effect of the anode grid upon background conditions. Potential distributions are shown in figure 11 for the plane bisecting the third band of apertures from the open cathode end in each case, using 24 evenly-spaced equipotential contours. Where the anode grid is included in the set-up (figure 11(i)) much of the potential is concentrated in a strong, relatively uniform radial field between the electrodes. In contrast, for the arrangement with cathode grid only (figure 11(ii)) the potential falls smoothly from the cathode radius, with some distortion as contours approach corners of the chamber. In both distributions, some potential is also dropped through the electrode apertures, causing curved equipotential surfaces that project away from the inter-electrode field. This distortion is particularly evident for the arrangement with the anode grid, where over 10% of full potential falls within the apertures of each electrode. In this case, the magnitude of distortion around the cathode apertures is increased, compared with the distribution surrounding the cathode only. The direction of electric field is normal to the contours in figure 11, and so the curved surfaces shown around the electrode apertures

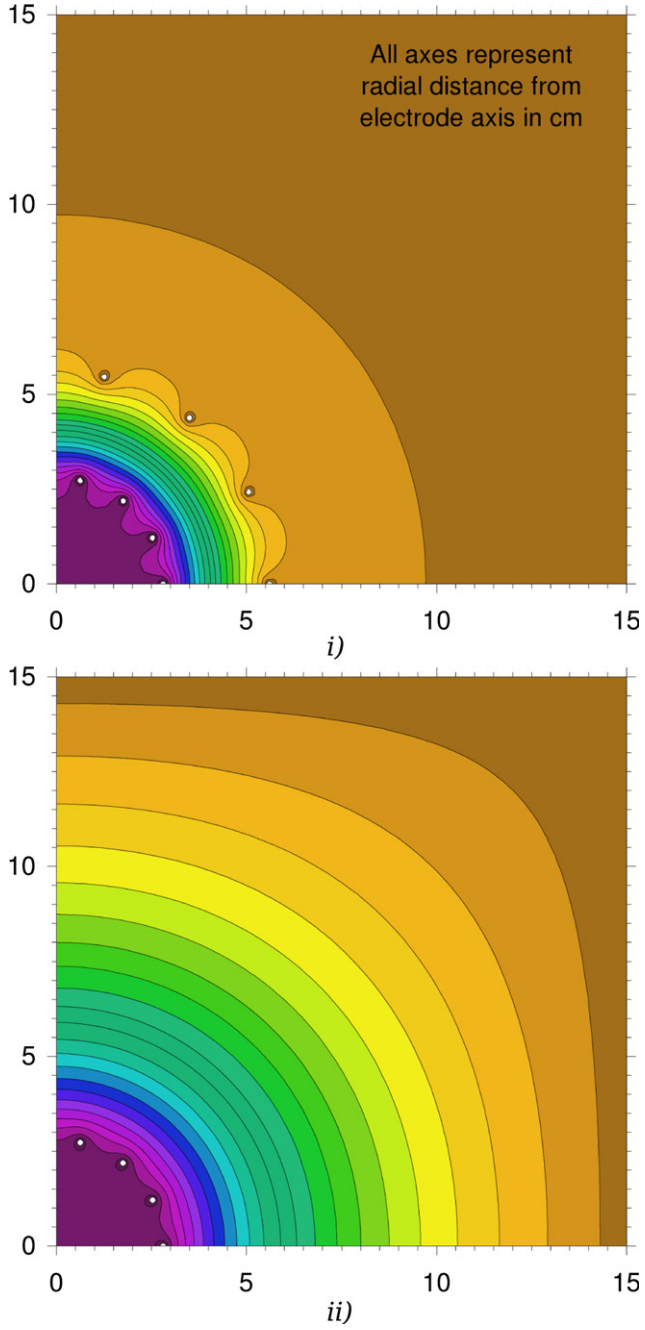

Figure 11. Radial potential distributions in vacuum, calculated for plane centred within the third band of cathode apertures from the open end. 24 evenly-spaced contours are shown, for set-ups with (i) anode and cathode, (ii) cathode only.

will cause an electrostatic lensing effect for charged particles, that may be focussing or defocussing according to direction of travel. The anode grid is seen to introduce a background field distribution that would focus positive species drifting inward through the apertures towards a steep accelerating gradient. Should this remain so in operation, radial ion beams might be formed across the inter-electrode region, and fluxes of fast neutrals produced by these would follow suitable trajectories for causing the observed distributions of emission.

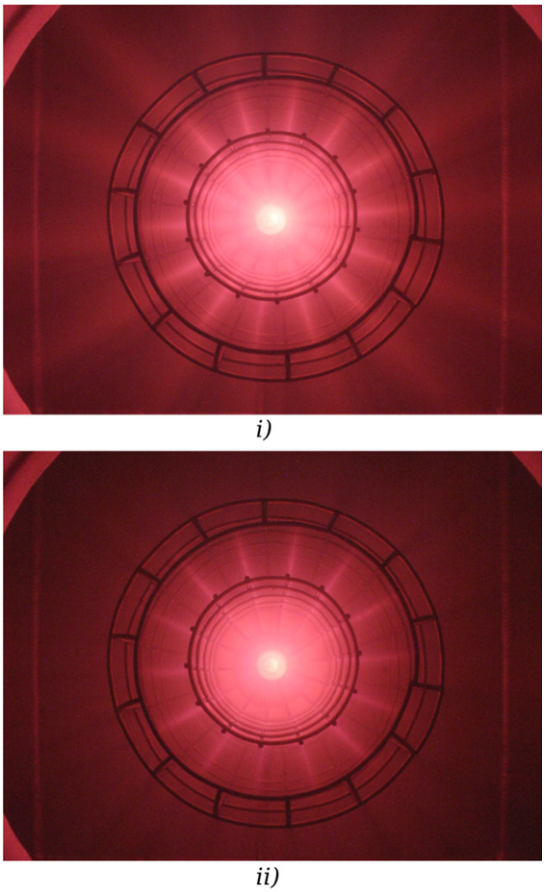

Figure 12. Beam mode discharges in neon, at constant cathode current of 2 mA, and pressure of $p = 1.5$ Pa, in (i) the standard arrangement where apertures of anode and cathode are radially aligned, and (ii) rotated cathode configuration, where these are out of phase.

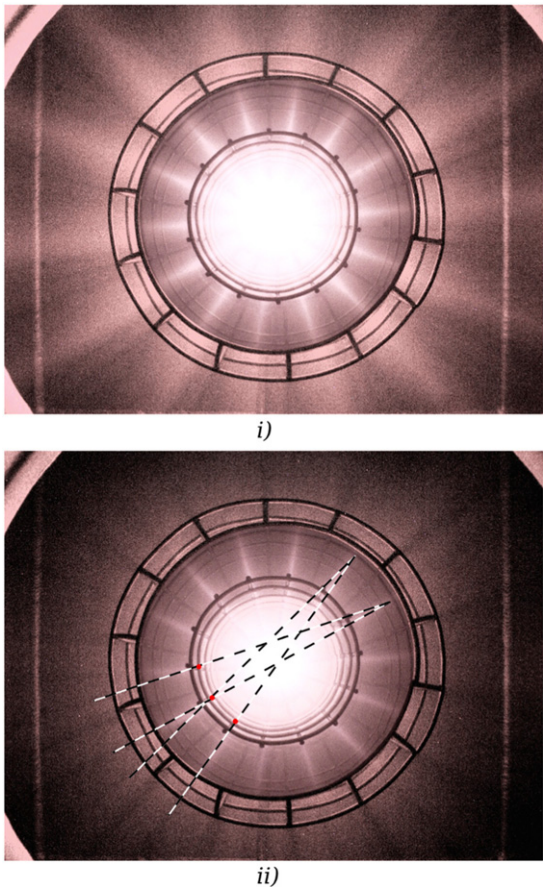

Figure 13. Images of neon discharges reproduced from figures 12 (i) and (ii), with contrast levels enhanced as described in the text. Black and white dashes in (ii) illustrate geometry of shadows cast by longitudinal members of the cathode marked with red spots.

3.3. Emission distributions in modified electrode arrangements

Processes causing the beam mode pattern of emission were further investigated by making a series of alterations to the experimental set-up, and then observing the effect upon emission when discharges were operated at usual beam mode conditions. Pressure, voltage and current were noted, but the discharges were not otherwise studied in detail. In the following we describe the results of several experiments that used the electrode arrangements illustrated in figure 2.

3.3.1. Anode removed. In a first simple modification to the standard apparatus, the anode grid was removed from the set-up, and discharges then operated over a range of pressures $p = 3.3$–6.4 Pa, with which the beam mode is generally associated in the standard set-up.

For all of these conditions, a diffuse distribution of emission occurred within and around the cathode, but no radial beams were evident. The predominant colour of emission in helium was pink-orange, similar to that shown in figure 9. This result demonstrates the anode to be required in the set-up for the beam pattern to appear.

3.3.2. Rotated cathode configuration. The influence of the anode grid was further explored using the 'rotated cathode' configuration shown in figure 2(ii), in which alignment between apertures of the anode and cathode was altered so as to interrupt the paths along which beam mode emission usually occurs. Distributions of emission were observed for discharges operated in both this and the standard configuration, at conditions of similar pressure and current. These discharges were operated at the supply limit of 2 mA current, using neon at a pressure $p = 1.5$ Pa as the background gas. At these conditions, cathode voltage was around 3.8 kV for the discharge in the standard set-up, and around 4.5 kV for the rotated configuration.

Figure 12 shows photographs of the discharges in (i) standard, and (ii) rotated cathode configurations. In both cases, the camera, exposure settings and perspective used were identical. In the standard set-up shown in figure 12(i) the distribution of emission appears generally similar to the helium example in section 3.2. With the rotated cathode configuration, figure 12(ii), radial lines of bright emission are still evident in the inter-electrode region, that remain aligned with the distribution of anode grid apertures. For this case, the beam pattern is largely absent in locations external to the anode radius, where emission appears generally less bright, and where some

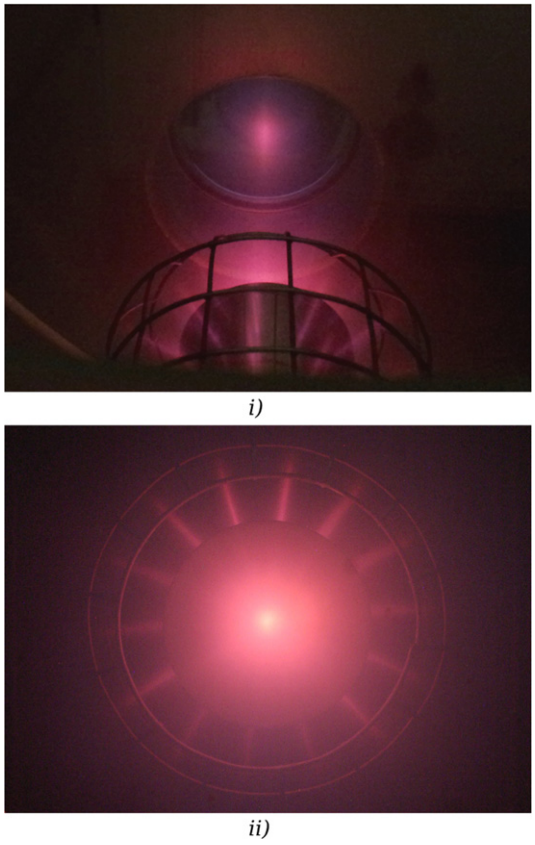

Figure 14. Discharge with anode grid and solid cathode, in neon at 2.4 Pa; 4.9 kV, 2 mA. (i) Perspective from above cathode feed-through, (ii) axial perspective.

dark lines are also evident. To clarify these, levels of contrast were enhanced, making identical adjustments to both images from figure 12. Due to variation in brightness, regions within the end ring of the anode were treated differently to the surrounds. Results for the standard arrangement (figure 13(i)) show similar pairs of lines, less well-defined than for helium but separated by a comparable angle of divergence, appearing projected from wires of the anode. For the discharge with rotated cathode, shown in figure 13(ii), the twin lines from wires of the anode grid are much less evident, and additional radially-oriented lines of dark space are distributed around the anode circumference. We have again followed the orientation of some dark lines using black and white dashes in figure 13(ii), in this instance showing only trajectories that intercept longitudinal wires of the cathode. These are seen to include many of the lines in the distribution, which are generally oriented to again converge within opposing apertures of the anode grid.

The pattern of emission observed in the rotated cathode set-up shows that where apertures of anode and cathode follow different radial alignments, the anode apertures determine the distribution of bright inter-electrode lines, and the beam-like elements causing the shadowed emission also remain aligned with these. In this case the beams significantly impact wires of the cathode, causing a direct effect upon the distribution of shadows. This obstruction by the cathode seems to also result in the general attenuation of the beam pattern of emission in locations beyond the anode radius, and indistinct double shadowing from wires of the anode.

3.3.3. Solid cathode configuration. The extent to which the beam pattern of emission might be independent of the grid cathode was tested with the 'solid cathode' configuration shown in figure 2(iii). A discharge was operated in this apparatus at a pressure of $p = 2.4$ Pa in neon, at conditions of $I_C = 2$ mA with cathode voltage $V_C = 4.9$ kV. Photographs in figure 14 show the distribution of emission observed for this discharge, from above the cathode feed-through, and from the axial perspective. A radial beam pattern of emission was observed in the annular region between the electrodes, in which one beam was aligned with each aperture of the anode. Diffuse axial emission also occurred around the end of the cathode and viewport, which partially obscure the distribution when viewed axially (figure 14(ii)). Regions elsewhere in the chamber were observed to be relatively dark.

The continued appearance of the beam pattern of emission in this set-up shows the anode to be fundamental for causing this, while the surface of the cathode is seen to be unimportant. The solid surface of the cathode however appears to largely prevent emission in the region surrounding the electrodes.

3.3.4. Planar electrode configuration. In a final experiment, the emission distribution was observed for a 'planar' electrode configuration, in which a flat cathode grid was sandwiched between two identical anode grids, as illustrated in figure 2(iv). The planar arrangement was operated in helium at a pressure of $p = 5.3$ Pa, with $V_C = 4$ kV and $I_C = 8$ mA. In figure 15, a photograph of this discharge shows emission distributed in a series of beam-like lines that are aligned normally to the plane of the electrodes, with a single beam passing through each set of apertures. The beams appear brighter within the two inter-electrode regions, although the pattern is also evident in the region to the side of the assembly. This is visible in the lower part of figure 15, where line of sight coincides with the orientation of aperture rows. The visible colour of emission in helium was pink-orange at these conditions.

The results of these experiments show how a grounded anode grid can create a beam-like pattern of emission in various different electrode configurations, that is further shown to consist of distinct components with different dependences; the bright lines between the electrodes that depend upon the distribution of anode grid apertures, and the less well-defined beams aligned with these that require clear pathways through the cathode to extend across the chamber. This effect of the anode grid is consistent with beams of ions being formed by potential surfaces around its apertures, similar to those shown in figure 11(i), as was discussed in section 3.2. This mechanism is considered to cause the beam-like form of discharge observed in all the various configurations tested, since such potential distributions may be expected to occur generally where a wire grid creates a boundary between regions of strong and weak fields.

The shadowing effects observed with the grid cathode arrangements suggest emission surrounding the anode to significantly result from excitation caused by fast neutrals, that

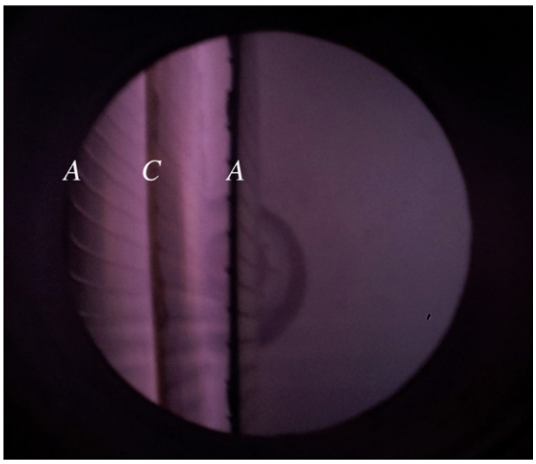

Figure 15. Discharge with planar grids in helium at 5.3 Pa; 4 kV, 8 mA. The perspective is mostly normal to the grid planes, and so similar to that of the diagram in figure 2(iv), with the letters A and C again denoting anode and cathode. The central, dark vertical line in the image is the edge of one anode grid, to the left of which are the cathode and other anode. The cathode feed-through is visible in the background.

have been produced within the inter-electrode beams and crossed the chamber through the cathode. This is in agreement with the consideration of spectral emission in section 3.1. The relative absence of such emission observed with the solid cathode is consistent with the obstruction of such radial pathways by the cathode surface. Significance of these neutrals for discharge operation is indicated by the variation in discharge perveance observed for the standard and rotated cathode arrangements, in which greater voltage and/or pressure was required for driving a fixed current for increasing obstruction of pathways through the electrode assembly. This seems likely to also explain the difference observed for the solid cathode arrangement, although additional effects of removing the hollow space within the cathode cannot be discounted. The apparent relation between discharge efficiency and free paths for fast neutrals is consistent with the contribution to ionisation these are expected to make, from broad similarities with excitation, and also from modelling of helium breakdown in a 2D representation of our standard cylindrical apparatus [62], that found ionisation by ions and neutrals to become important for helium pressures below 7 Pa, with the contribution by electrons smaller below 6 Pa.

4. Discussion

Optical emission from the beam mode indicates the discharge to be significantly composed of convergent beams of energetic ions and neutrals, created by a focussing effect of the grounded anode grid that was observed to operate in other electrode geometries also.

For context, we first consider how these characteristics compare with those of the IEC star mode. Both discharges create a radial beam pattern of emission, but star mode beams or 'microchannels' occur in devices with no anode grid, and are rather formed by effects of particles diverging from the cathode apertures [10, 13]. Various measurements of star mode microchannels [19, 20, 29, 43] have shown the ion motion in these to also be principally divergent, accelerated outwards from within the cathode with little or no evidence for convergent flow. A 'hollow cathode' model [43] has proposed significant ionisation to occur due to electrostatic confinement of electrons within the cathode, and this to cause microchannels as ions are accelerated away from a virtual anode at the centre, that measurements indicate to be around a quarter of cathode potential in height [43, 63]. While details of electron diffusion from such a configuration are unclear, we have observed hollow cathode electron confinement to benefit from more evenly-enclosed grid cathodes [2], and confined electrons will still contribute to ionisation at conditions where this is insufficient to fully sustain the discharge. Even in our open-ended cathode, we expect this electron confinement may be responsible for the electron-impact element of beam mode emission described in section 3.1.

If the divergent model is generally representative of the star mode, then the convergent beam mode may be unique among IEC glow discharges. It is interesting to consider an example of a star mode discharge in which a grounded anode grid did not produce converging beams [18]; this was observed in a similarly cylindrical arrangement of anode and cathode grids, that were constructed from longitudinal wires only, with twice as many used for the anode. Focussing potential distributions would still be expected to occur around these wires, but a photograph of a star mode discharge in grounded-anode configuration shows the number and spatial arrangement of beams to follow the distribution of cathode apertures, rather than those of the anode. It seems the determining factor behind this must be some difference in properties between the two sets of apparatus, and it is only our set-up that has the available axial space beyond the electrodes that allows electrons to escape from the open cathode end. This further supports the hollow cathode model of the star mode, and suggests the short length and open end of our cathode may be critically important for determining the discharge configuration, as well as the focussing effect of the anode grid.

From a practical point of view, the different spatial distributions of ionisation implied for divergent and convergent beams may result in quite different discharge properties. The convergent ion flow in the beam mode suggests a large ionisation component in the outer region between grounded anode and chamber wall, where local potential is expected to be generally closer to chamber ground than to the cathode, and more discharge energy is available to ions and neutrals than to electrons. Such a configuration will be more efficient for creating energetic heavy species, suggesting the beam mode may be generally favourable for this. Another practical effect of the anode grid in our set-up is to significantly increase the strength of background electric field within the chamber (figure 11), that is likely to moderate the voltage required for generating a given range of ion and neutral energies.

For IEC discharge work, where beam-background collisions are known to dominate fusion reactivity [12, 64], the convergent beam model may be a more efficient means of

producing energetic ions and neutrals. We were not able to measure particle energies from a beam mode discharge, or to conduct any fusion experiments, but future research might determine whether these apparent differences to star mode translate into enhanced performance. The grid-focussing effect we observed at discharge conditions will also operate at lower pressures, where ion flow can recirculate through an IEC cathode, and where ion sources are often placed peripherally e.g. references [18, 24, 25, 30]. Our observations illustrate the importance of good grid alignment where multiple electrodes are used, as has been demonstrated for more complicated arrangements in spherical geometry [16, 17, 21].

For plasma source applications, a discharge in which ions and neutrals are significantly energetic is likely to create a different environment to those of electron-driven plasmas. The emission structure observed for the beam mode in section 3.1 provides an example of how collisional processes can depend significantly upon energetic species, as interactions possible in a quasi-molecular state formed in ion and neutral collisions result in a different distribution of excitation [53, 58]. The molecular and anionic chemistry produced in TCDs in hydrogen species also shows a dependence upon operating conditions [65, 66], with increasing diversity expected for more complex molecular fill species. In the discharge regime, the ion mean-free path is generally a fraction of the ion transport distance and frequent collisions will produce large numbers of fast neutrals. This is demonstrated by emission in the beam mode, that also shows how neutrals may propagate throughout the chamber to cause collisional processes remotely from the source.

The beam emission patterns observed in different electrode arrangements indicate an anode-focussed ion beam discharge may be created in diverse geometries. Further observations are required to characterise the planar discharge, but might show this to be a versatile implementation that can avoid the hollow cathode instability. This might also be further manipulated to create various convergences of neutral beams, as described in references [39, 40, 67] for a single perforated cathode immersed in a background plasma, that produced beams suitable for dielectric materials processing. In comparison with this approach, the simplicity of an entirely self-sustained discharge might not compensate for the constraints upon operating range, but addition of a focussing anode could offer additional control over properties of the beam produced.

5. Conclusions

In this study we described optical emission from a glow discharge we call the beam mode, that occurs in a nested arrangement of cylindrical grid electrodes in which an open-ended hollow cathode is surrounded by a grounded anode.

When we compared measurements of helium spectral emission from the beam mode and a hollow cathode mode against simple models for impact excitation by ions and neutrals, and by electrons, the results suggested the sampled beam mode emission was caused significantly by fast neutrals, but to also contain a large component caused by electrons.

We also considered the spatial distribution of this emission, a series of radial beams that pass through aligned apertures of anode and cathode and extend to the chamber walls. We observed a distinctive shadowing effect caused by wires of the electrodes, that indicates the pattern to be caused as radially-convergent beams of ions cross the inter-electrode region, and produce co-linear beams of fast neutrals that propagate across the chamber. Calculated background potential distributions show an electrostatic focussing effect for apertures of the anode grid, that indicates these will form beams from inwardly drifting ions.

The relation between the beam-like emission distribution and the electrode arrangement was investigated by observing emission for discharges created in a series of different electrode assemblies at beam mode conditions, including a parallel-planar assembly. These produced emission distributions with elements characteristic of excitation by ions and by neutrals; bright radial beams crossing the inter-electrode region that appear to rely upon electrostatic focussing by the potential distribution surrounding apertures of the anode grid, and co-linear beams that propagate through clear pathways within the chamber unaffected by electric fields.

These observations show the beam mode to be an anode-focussed ion beam discharge, that creates significant fluxes of fast neutrals by charge exchange and momentum transfer collisions. Although superficially resembling the star mode described elsewhere in the IEC literature, the beam mode is distinguished by the focussing effect of the anode grid, and so constitutes a novel mode of IEC discharge operation.

Acknowledgements

This work was supported by the Engineering and Physical Sciences Research Council, grant reference EP/L505018/1.

Data availability statement

The data that support the findings of this study are available upon reasonable request from the authors.

ORCID iDs

T Hardiment https://orcid.org/0000-0001-8217-0182
M D Bowden https://orcid.org/0000-0003-4128-4823

References

[1] Hardiment T and Bowden M D 2019 *IEEE Trans. Plasma Sci.* **47** 3124–33
[2] Hardiment T and Bowden M D 2020 *Phys. Plasmas* **27** 043506
[3] Lavrent'ev O, Ovcharenko L, Safronov B, Sidorkin V and Nemashkalo B 1963 *Ukr. Fiz.* **8** 440–5
[4] Farnsworth P T 1966 *US Patent* 3258402
[5] Elmore W C, Tuck J L and Watson K M 1959 *Phys. Fluids* **2** 239–46
[6] Hirsch R L 1967 *J. Appl. Phys.* **38** 4522–34

[7] Nadler J H, Miley G H, Gu Y and Hochberg T 1992 *Fusion Technol.* **21** 1639–43
[8] Miley G H, Javedani J, Yamamoto Y, Nebel R, Nadler J, Gu Y, Satsangi A and Heck P 1994 Inertial electrostatic confinement neutron/proton source dense Z-pinches *3rd Int. Conf.* (New York: AIP) pp 675–89
[9] Anderl R, Hartwell J, Nadler J, DeMora J, Stubbers R and Miley G 1995 Development of an IEC neutron source for NDE *Proc. 16th Int. Symp. Fusion Engineering* vol 2 (Piscataway, NJ: IEEE) pp 1482–5
[10] Miley G H, Yibin Gu Y, Demora J M, Stubbers R A, Hochberg T A, Nadler J H and Anderl R A 1997 *IEEE Trans. Plasma Sci.* **25** 733–9
[11] Miley G H and Sved J 2000 *Appl. Radiat. Isot.* **53** 779–83
[12] Thorson T A, Durst R D, Fonck R J and Sontag A C 1998 *Nucl. Fusion* **38** 495
[13] Ohnishi M, Hoshino C, Masuda K, Yamamoto Y, Toku H and Yoshikawa K 1999 Electron streaming from central core region in inertial-electrostatic confinement fusion *18th Symp. Fusion Engineering* (Piscataway, NJ: IEEE) pp 213–6
[14] Yoshikawa K *et al* 2001 *Nucl. Fusion* **41** 717
[15] Weidner J W, Kulcinski G L, Santarius J F, Ashley R P, Piefer G, Cipiti B, Radel R and Murali S K 2003 *Fusion Sci. Technol.* **44** 539–43
[16] McGuire T J and Sedwick R J 2005 *J. Propul. Power* **21** 697–706
[17] Sedwick R, McGuire T, Dietrich C, Warner N and Zayas D 2006 Multi-grid IEC fusion for space power and propulsion *42nd AIAA/ASME/SAE/ASEE Joint Propulsion Conf. Exhibit* p 4390
[18] Yamauchi K, Ohura S, Watanabe M, Okino A, Kohno T, Hotta E and Yuura M 2006 *IEE J. Trans. Fundam. Mater.* **126** 1177–82
[19] Shrier O, Khachan J, Bosi S, Fitzgerald M and Evans N 2006 *Phys. Plasmas* **13** 012703
[20] Khachan J and Samarian A 2007 *Phys. Lett.* A **363** 297–301
[21] Dietrich C, Sedwick R and Eurice L 2008 Experimental verification of enhanced confinement in a multi-grid IEC device *44th AIAA/ASME/SAE/ASEE Joint Propulsion Conf. Exhibit* p 4760
[22] Meyer R M, Prelas M A and Loyalka S K 2008 *IEEE Trans. Plasma Sci.* **36** 1881–9
[23] Taniuchi Y, Matsumura Y, Taira K, Utsumi M, Chiba M, Shirakawa T and Fujii M 2010 *J. Nucl. Sci. Technol.* **47** 626–33
[24] Masuda K, Nakagawa T, Kipritidis J, Kajiwara T, Yamagaki Y, Zen H, Yoshikawa K and Nagasaki K 2010 *Plasma Phys. Control. Fusion* **52** 095010
[25] Murali S K, Santarius J F and Kulcinski G L 2010 *J. Fusion Energy* **29** 141–5
[26] Kulcinski G L *et al* 2011 *Fusion Sci. Technol.* **60** 607–14
[27] Kulcinski G L *et al* 2015 *Fusion Sci. Technol.* **68** 314–8
[28] Buzarbaruah N, Dutta N J, Borgohain D, Mohanty S R and Bailung H 2017 *Phys. Lett.* A **381** 2391–6
[29] Ranson N, Pigeon V, Claire N and Khachan J 2020 *Phys. Plasmas* **27** 103501
[30] Bhattacharjee D, Buzarbaruah N, Mohanty S and Adhikari S 2020 *Phys. Rev.* E **102** 063205
[31] Bakr M, Mukai K, Masuda K, Yagi J and Konishi S 2021 *Fusion Eng. Des.* **167** 112346
[32] Rao M V V S, Van Brunt R J and Olthoff J K 1996 *Phys. Rev.* E **54** 5641
[33] Hartmann P, Donkó Z, Bánó G, Szalai L and Rózsa K 2000 *Plasma Sources Sci. Technol.* **9** 183
[34] Hartmann P, Matsuo H, Ohtsuka Y, Fukao M, Kando M and Donkó Z 2003 *Japan. J. Appl. Phys.* **42** 3633
[35] Jelenković B and Phelps A 2005 *Phys. Rev.* E **71** 016410
[36] Xu L and Wang H 2018 *J. Phys. D: Appl. Phys.* **51** 335206
[37] Xu L, Khrabrov A V, Kaganovich I D and Sommerer T J 2018 *Plasma Sources Sci. Technol.* **27** 104004
[38] Blackhall L and Khachan J 2007 *J. Phys. D: Appl. Phys.* **40** 2491
[39] Grigoriev S N, Melnik Y A, Metel A S and Volosova M A 2017 *J. Appl. Phys.* **121** 223302
[40] Grigoriev S, Metel A, Melnik Y and Volosova M 2018 *Machines* **6** 58
[41] Grigoriev S N, Melnik Y A and Metel A S 2013 *Instrum. Exp. Tech.* **56** 358–64
[42] Wulfkuehler J P and Tajmar M 2016 Novel inertial electrostatic confinement fusion with buckyball-shaped multi-grids *52nd AIAA/SAE/ASEE Joint Propulsion Conf* p 4777
[43] Hermens J, Jaspers R and Khachan J 2019 *Phys. Plasmas* **26** 102703
[44] Arslanbekov R R, Kudryavtsev A A and Tobin R C 1998 *Plasma Sources Sci. Technol.* **7** 310
[45] Kolobov V I and Metel A S 2015 *J. Phys. D: Appl. Phys.* **48** 233001
[46] Jobe J D and John R M 1972 *Phys. Rev.* A **5** 295
[47] Phelps A V 1958 *Phys. Rev.* **110** 1362
[48] John R M S and Fowler R G 1961 *Phys. Rev.* **122** 1813
[49] Sovie R J 1964 *Phys. Fluids* **7** 613–4
[50] De Vries R F and Mewe R 1966 *Phys. Fluids* **9** 414–5
[51] Hagelaar G J M, Mihailova D B and Van Dijk J 2010 *J. Phys. D: Appl. Phys.* **43** 465204
[52] Ralchenko Y, Janev R K, Kato T, Fursa D V, Bray I and De Heer F J 2008 *At. Data Nucl. Data Tables* **94** 603–22
[53] Okasaka R, Konishi Y, Sato Y and Fukuda K 1987 *J. Phys. B: At. Mol. Phys.* **20** 3771
[54] De Heer F J and Van den Bos J 1965 *Physica* **31** 365–84
[55] De Heer F J, Wolterbeek Muller L and Geballe R 1965 *Physica* **31** 1745–55
[56] Tani M, Hishikawa A and Okasaka R 1991 *J. Phys. B: At. Mol. Opt. Phys.* **24** 1359
[57] Kurskov S Y and Khakhaev A D 2006 *Czech. J. Phys.* **56** 297B–302
[58] Kempter V, Veith F and Zehnle L 1975 *J. Phys. B: At. Mol. Phys.* **8** 1041
[59] Kempter V, Riecke G, Veith F and Zehnle L 1976 *J. Phys. B: At. Mol. Phys.* **9** 3081
[60] Hayden H C and Utterback N G 1964 *Phys. Rev.* **135** A1575
[61] Gilbody H and Hasted J 1957 *Proc. R. Soc.* A **240** 382–95
[62] Al-Khateeb A 2018 A modelling study of transparent cathode discharge breakdown *PhD Thesis* University of Liverpoo
[63] Khachan J, Moore D and Bosi S 2003 *Phys. Plasmas* **10** 596–9
[64] Bowden-Reid R, Khachan J, Wulfkühler J-P and Tajmar M 2018 *Phys. Plasmas* **25** 112702
[65] Fitzgerald M, Khachan J and Bosi S 2006 *Eur. Phys. J.* D **39** 35–9
[66] Boris D R *et al* 2009 *Phys. Rev.* E **80** 036408
[67] Metel A S 2012 *Plasma Phys. Rep.* **38** 254–62